Journal of Computational Physics 227 (2008) 9807–9822

Contents lists available at ScienceDirect

Journal of Computational Physics

journal homepage: www.elsevier.com/locate/jcp

A multiscale reduced-basis method for parametrized elliptic partial differential equations with multiple scales

N.C. Nguyen *

Department of Aeronautics and Astronautics, Massachusetts Institute of Technology, Rm 37-435, 77 Massachusetts Avenue, Cambridge, MA 02139, United States

ARTICLE INFO

Article history:
Received 20 October 2007
Received in revised form 20 July 2008
Accepted 21 July 2008
Available online 19 August 2008

Keywords:
Multiscale
Homogenization
Reduced basis
Finite element
Galerkin approximation

ABSTRACT

We present a technique for solving parametrized elliptic partial differential equations with multiple scales. The technique is based on the combination of the reduced basis method [C. Prud'homme, D. Rovas, K. Veroy, Y. Maday, A.T. Patera, G. Turinici, Reliable real-time solution of parametrized partial differential equations: reduced-basis output bound methods, Journal of Fluids Engineering 124 (1) (2002) 70–80] and the multiscale finite element method [T.Y. Hou, X.H. Wu, A multiscale finite element method for elliptic problems in composite materials and porous media, Journal of Computational Physics 134 (1) (1997) 169–189] to treat problems in which the differential coefficient is characterized by a large number of independent parameters. For the multiscale finite element method, a large number of cell problems has to be solved at the fine local mesh for each new configuration of the differential coefficient. In order to improve the computational efficiency of this method, we construct reduced basis spaces that are adapted to the local parameter dependence of the differential operator. The approximate solutions of the cell problems are computed accurately and efficiently via performing Galekin projection onto the reduced basis spaces and implementing the offline–online computational procedure. Therefore, a large number of similar computations at the fine local mesh can be carried out with lower computational cost for each new configuration of the differential coefficient. Numerical results are provided to demonstrate the accuracy and efficiency of the proposed approach.

1. Introduction

Many real problems of fundamental and practical importance are multiscale, possessing several macroscopic phases or dissimilar constituents. Typically, for two-scale problems, the microscopic component is dispersed as particles or inclusions in a continuous matrix of the macroscopic component. Representative multiscale systems in mechanics are composite materials, porous media, sedimenting suspensions and fluidized beds, and turbulent phenomena in high Reynolds number flows. Composite materials are used in a variety of applications such as aircraft industry, wind turbine blades, thermal insulators or conductors. Fibrous porous media are encountered in groundwater transport [11], manufacturing applications [12], environmental and filtration system [10], and biological processes [18].

We consider here multiscale problems that are modeled by elliptic partial differential equations (PDE) which have the differential coefficients depending not only on the spatial coordinates but also on a large number of parameters. Such problems often arise in multiscale modeling and analysis in porous media and composite materials, where we would like to perform analysis of the porous flows for different permeability configurations or optimization/design of the composite materials. These problems typically require repetitive simulations of the underlying PDEs for many different configurations

* Tel.: +1 617 253 8080.
E-mail address: cuongng@mit.edu

0021-9991/$ - see front matter © 2008 Elsevier Inc. All rights reserved.
doi:10.1016/j.jcp.2008.07.025

of the differential coefficient as a function of the parameters. It is therefore of considerable interest to develop a dedicated method for such applications.

The complete analysis of multiscale systems is an extremely difficult task. Direct numerical solutions of flow and transport in porous media have been reported in the literature [2,7,32]. These results reveal detailed information of the physical processes at all scales. Unfortunately, due to the enormous amount of CPU time and computer memory required to accommodate the scale of computation, direct numerical methods are not suitable for repeated simulations. From an engineering perspective, the prediction of the macroscopic properties of the multiscale systems, such as thermal conductivity, elastic moduli, and permeability, generally suffices. Therefore, many researchers focus on the development of techniques that capture the small scale effect on the large scales without resolving all the small scale features.

In [9], Cruz and Patera propose a parallel Monte-Carlo finite element (FE) procedure for the analysis of multiscale random media. The original multiscale problem is recast as a sequence of three scale-decoupled subproblems in which the computationally intensive mesoscale subproblem is repeatedly solved by parallel nested Monte-Carlo and finite-element methods. The multiscale FE method introduced by Hou et al. [15,16] has been successfully applied to multiscale elliptic problems. The main idea is to construct FE basis functions which capture the small scale information within each element. The small scale information is then transferred to the large scales through the coupling of the global stiffness matrix. Hence, the effect of small scales on the large scales is correctly captured. The multiscale FE methods have the ability to solve multiscale problems with accuracy comparable to the direct numerical simulation at the fine grid, while reducing the storage requirements quite significantly. The multiscale FE methods are extremely efficient for solving problems for different source terms and boundary conditions. However, when applied to solve problems for different media, the multiscale FE methods have the operation count comparable to the direct FE methods. Other methods such as the multiscale finite volume method [17] and the mixed multiscale FE method [8] suffer from a similar drawback.

In this paper, we introduce a multiscale reduced-basis method for solving a class of parametrized elliptic problems with multiple scales. Our approach is based on the combination of the RB method [4,13,25,24,27,29,30] for parametrized (monoscale) elliptic PDEs and the multiscale FE method [15,16] for multiscale elliptic PDEs. The main idea of the RB method is to represent the solution of parametrized PDEs by a small set of basis functions which is referred as reduced basis. The reduced basis is constructed from a larger set of snapshots which are typically pre-computed solutions of the underlying PDE at selected parameter points. The reduced basis is thus adapted to the local parameter dependence of the differential operator. As a consequence, the size of the original problem can be significantly reduced since only a small number of basis functions is typically required. We apply this RB recipe to treat the cell problem: first, we construct the reduced basis by using an adaptive sampling procedure introduced in [24]; we then perform a Galekin projection of the cell problem onto the reduced basis space to obtain a reduced order model; finally, in order to efficiently evaluate the reduced order model, we implement the offline–online procedure which splits the computational process into offline and online stages. The offline stage – performed only once for generating the reduced order model – is typically expensive. However, the operation count of the online stage – performed many times for simulating the reduced order model – depends only on the dimension of the reduced basis and the parametric complexity of the cell problem.

When applied to multiscale parametrized elliptic PDEs, the RB method offers several attractive features. First, the method results in a reduced model that may have significantly less degrees of freedom than the corresponding FE model for solving the cell problems. As a result, the computational time for repeated solution of the parametrized elliptic PDEs with multiple scales can be substantially reduced. Second, the method allows for a high resolution of the microscopic scale to achieve higher accuracy without increasing the online computational cost. Third, the method needs the same computer memory as the multiscale FE methods. And fourth, like the multiscale FE methods, the multiscale RB method is highly parallelizable since the computation on each cell problem is carried out independently. However, as mentioned earlier, its major drawback is due to the computationally intensive offline stage. Fortunately, for certain problems in which the differential coefficients have a similar parametrized form on each element, the computational cost of the offline stage is relatively small. The multiscale RB method is well-suited for such problems.

The remainder of the paper is organized as follows. In Section 2, we formulate the continuous problem and describe two popular solution approaches, namely the homogenization methods and the multiscale methods. In Section 3, we describe the RB method for rapid solution of parametrized elliptic PDEs with multiple scales. In Section 4, we discuss the results obtained for a single phase flow through random porous media. Finally, in Section 5, we present concluding remarks.

2. Problem formulation and numerical methods

2.1. Parametrized elliptic PDEs with multiple scales

We consider parametrized second-order elliptic problems of the form

$$-\nabla \cdot (g(\boldsymbol{x};\boldsymbol{\mu})\nabla u) = f(\boldsymbol{x}) \quad \text{in } \Omega, \tag{1}$$

where Ω is a bounded domain in $\mathbb{R}^{d=2}$ with Lipschitz boundary $\partial\Omega$, f is a source term; and g is a nonnegative scalar coefficient which depends on $\boldsymbol{x} = (x, y) \in \Omega$ and $\boldsymbol{\mu}$. Here $\boldsymbol{\mu}$ is a large set of parameters which take random values in some range. For heat conduction in composite materials, u and g represent temperature and thermal conductivity, respectively. For single phase

flows in porous media, u is the pressure and $g = p/v$ is the ratio of the permeability p and the fluid viscosity v. In many cases, g may be random or highly oscillatory in $\boldsymbol{x}$, but vary quite smoothly in $\boldsymbol{\mu}$. Thus the solution of (1) displays a multiple scale structure, but in general well behaves with respect to variation in $\boldsymbol{\mu}$. For simplicity of presentation, we consider scalar differential coefficients, although tensorial coefficients can be treated in a similar way.

We introduce some notation. First we denote by $L^2(\Omega)$ the space of square integrable functions defined in Ω with inner product

$$(w, v)_0 = \int_\Omega wv \, \mathrm{d}\Omega \tag{2}$$

and induced norm $\|v\|_0 = \sqrt{(v, v)_0}$. Then $H^1(\Omega) = \{v \in L^2(\Omega) \,|\, \nabla v \in (L^2(\Omega))^2\}$ is the Hilbert space with inner product

$$(w, v)_1 = \int_\Omega wv + \nabla w \cdot \nabla v \, \mathrm{d}\Omega \tag{3}$$

and induced norm $\|v\|_1 = \sqrt{(v, v)_1}$. $H_0^1(\Omega)$ consists of functions in $H^1(\Omega)$ that vanish on $\partial\Omega$.

For simplicity of exposition, we assume that $u = 0$ on $\partial\Omega$. The variational formulation is to seek $u \in H_0^1(\Omega)$ such that

$$a(u, v; \boldsymbol{\mu}) = \ell(v), \quad \forall v \in H_0^1(\Omega), \tag{4}$$

where

$$a(w, v; \boldsymbol{\mu}) = \int_\Omega g(\boldsymbol{x}; \boldsymbol{\mu}) \nabla w \cdot \nabla v \, \mathrm{d}\Omega, \quad \ell(v) = \int_\Omega f(\boldsymbol{x}) v \, \mathrm{d}\Omega. \tag{5}$$

A FE approximation $u_\mathrm{h} \in X_\mathrm{h}$ to u is then found as

$$a(u_\mathrm{h}, v; \boldsymbol{\mu}) = \ell(v), \quad \forall v \in X_\mathrm{h}, \tag{6}$$

where $X_\mathrm{h} \in H_0^1(\Omega)$ is a FE approximation space of dimension $\mathcal{N}$. The accuracy of the approximate solution u_h depends crucially on the basis set $\{\varphi_1, \ldots, \varphi_\mathcal{N}\}$ and the dimension $\mathcal{N}$ of X_h. For example, in the standard Galerkin FE method, basis functions are piecewise polynomials. For such polynomial basis functions, an attempt of directly solving (6) would require $\mathcal{N}$ extremely large in order to resolve the smallest scale ϵ of the problem. The computational demands become prohibitive as $\epsilon \to 0$.

The deficiency of direct numerical simulation leads to the development of homogenization methods and multiscale methods which we briefly describe below. For notational simplification, we shall drop the dependence of g on $\boldsymbol{\mu}$ in the remainder of this section.

2.2. Homogenization methods

To resolve the small scales, homogenization methods construct coarse-scale computational models in which small scale variations in the coefficients of the governing PDEs are homogenized and upscaled to the macroscopic scale. This process is often realized by making certain assumptions on the problem. In periodic homogenization, one assumes $g(\boldsymbol{y})$ to be periodic and smooth in the unit cubic $Y = [0, 1]^d$, where $\boldsymbol{y} = \boldsymbol{x}/\epsilon$ is the fast variable.

The homogenization theory [5] then states that the solution of (1) has an asymptotic expansion:

$$u \approx u^\star(\boldsymbol{x}) + \epsilon \sum_{i=1}^{d} \chi_i(\boldsymbol{x}/\epsilon) \frac{\partial u^\star(\boldsymbol{x})}{\partial x_i} - \epsilon \tilde{u}_1(\boldsymbol{x}) + O(\epsilon^2), \tag{7}$$

where the periodic functions $\chi_i(\boldsymbol{y}), 1 \leqslant i \leqslant d$, satisfy

$$-\nabla_y \cdot g(\boldsymbol{y}) \nabla_y \chi_i(\boldsymbol{y}) = \nabla_y \cdot g(\boldsymbol{y}) \boldsymbol{e}_i, \quad \text{in } Y, \tag{8}$$

and zero mean constraint for uniqueness

$$\int_Y \chi_j(\boldsymbol{y}) \mathrm{d}y = 0. \tag{9}$$

Here $u^\star$ is the solution of the homogenized problem

$$-\nabla \cdot \boldsymbol{g}^\star \nabla u^\star = f, \quad \text{in } \Omega, \qquad u^\star = 0 \quad \text{on } \partial\Omega, \tag{10}$$

where the constant effective tensor $\boldsymbol{g}^\star$ is given by

$$g_{ij}^\star = \int_Y g(\boldsymbol{y})[\boldsymbol{e}_i + \nabla_y \chi_j(\boldsymbol{y})] \cdot \boldsymbol{e}_j \mathrm{d}y. \tag{11}$$

Note $\boldsymbol{e}_i, 1 \leqslant i \leqslant d$, are the unit vectors. To account for the boundary condition $u|_{\partial\Omega} = 0$, the first order correction term $\tilde{u}_1$ is found such that

$$-\nabla \cdot g(\boldsymbol{x}/\epsilon) \nabla \tilde{u}_1 = 0, \quad \text{in } \Omega, \qquad \tilde{u}_1 = \sum_{i=1}^{d} \chi_i(\boldsymbol{x}/\epsilon) \frac{\partial u^\star(\boldsymbol{x})}{\partial x_i} \quad \text{on } \partial\Omega. \tag{12}$$

The detailed analysis of the asymptotic expansion (7) is given in [5,23]. Point-wise convergence of $u^\star$ to u as $\epsilon \to 0$ is obtained under certain smoothness conditions. For $L^2(\Omega)$ convergence, the conditions can be weakened.

Numerical homogenization strategies prove very attractive for periodic structures. Unfortunately, in the non-periodic case, although there still exist an homogenized problem and asymptotic expansion similar to (7), the effective tensor $\boldsymbol{g}^\star$ is unknown *a priori*. Therefore, one cannot replace the original problem (1) with the homogenized problem (10).

Recently, Allaire and Brizzi introduce a multiscale FE method [3] for numerical homogenization of non-periodic elliptic problems. Instead of assuming a constant value on the whole domain Ω, Allaire and Brizzi [3] suggest that the effective tensor $\boldsymbol{g}^\star$ is constant in each cell and determined by solving a large number of cell problems. The RB approach has also been successfully developed to compute the averaged coefficients for the homogenization of elliptic PDEs [6]. The basic idea is to parametrize the cell problem and develop its reduced order model. Boyaval demonstrates in his paper [6] that the RB approach significantly reduces the computational time in comparison with the FE method, albeit at locally periodic settings with piecewise affine oscillating coefficients.

2.3. Multiscale methods

Several multiscale methods such as the multiscale FE method [15,16], multiscale finite volume method [17], mixed multiscale FE method [8], and multiscale discontinuous Galerkin method [1] have been proposed for multiscale modeling and analysis. In these methods, one does not alter the differential coefficients, but instead one constructs coarse-scale approximation spaces that reflect subgrid structures in a way consistent with the local property of the differential operator. More precisely, the basis functions are computed as solutions of (a large number of) cell problems. This is in sharp contrast to the standard FE methods which employ piecewise polynomials. Typically, the multiscale methods result in more accurate solution than the standard FE methods for the same number of degrees of freedom thanks to the more adaptive basis functions. We briefly describe the multiscale FE method of Hou and Wu [15] to which we shall evaluate the performance of the multiscale RB method.

Let $\mathcal{Q}$ be a collection of elements $\Omega^k, 1 \leqslant k \leqslant K$, with diameter $\leqslant h$ such that $\overline{\Omega} = \bigcup_{\Omega^k \in \mathcal{Q}} \overline{\Omega}^k$ and $\Omega^k \cap \Omega^\ell = \emptyset$ for $k \neq \ell$. Here K denotes the number of elements. In each element Ω^k, we introduce a set of nodal basis $\{\phi^{ki}, i = 1, \ldots, n_e\}$ with n_e being the number of nodes of the element, where ϕ^{ki} satisfies

$$-\nabla \cdot g(\boldsymbol{x}) \nabla \phi^{ki} = 0, \quad \text{in } \Omega^k, \qquad \phi^{ki} = \sigma^{ki} \quad \text{on } \partial\Omega^k. \tag{13}$$

Here the functions σ^{ki}, $1 \leqslant i \leqslant n_e$, defined on $\partial\Omega^k$ play the role of Dirichlet boundary conditions. To ensure the continuity of the basis functions, we require that $\sigma^{ki} = \sigma^{\ell i}$, $1 \leqslant i \leqslant n_e$, across all non-degenerate interfaces $\Gamma_{k\ell} = \partial\Omega^k \cap \partial\Omega^\ell$. We then introduce the FE approximation space

$$Y_h = \text{span}\{\phi_H^{ki} : 1 \leqslant k \leqslant K, 1 \leqslant i \leqslant n_e\}, \tag{14}$$

where ϕ_H^{ki} is a FE approximation to ϕ^{ki}. The multiscale FE method now seeks $u_h^Y \in Y_h$ such that

$$a(u_h^Y, v) = \ell(v), \quad \forall v \in Y_h. \tag{15}$$

Since the basis functions are obtained by solving Kn_e cell problems (13), the approximation quality depends on the choice of boundary data σ^{ki}. The simplest choice is to let σ^{ki} vary linearly along $\partial\Omega^k$. Another more appealing choice which often leads to an improved accuracy is to assign σ^{ki} as the solution of reduced elliptic problems on each side of $\partial\Omega^k$.

In [15,16], using the homogenization theory discussed earlier, it was shown that

$$\|u - u_h^Y\|_1 \leqslant C_1 h \|f\|_1 + C_2 (\epsilon/h)^{\frac{1}{2}} \quad (\epsilon < h) \tag{16}$$

and

$$\|u - u_h^Y\|_0 = O(h^2 + \epsilon/h) \qquad (\epsilon < h). \tag{17}$$

The results imply that u_h^Y converges to the correct homogenized solution in the limit as $\epsilon \to 0$ in both $H^1(\Omega)$ and $L^2(\Omega)$ norms. However, they also reveal the resonance effect between the grid scale h and the small scale ϵ of the problem, i.e., the multiscale FE method attains a large resonance error in both $H^1(\Omega)$ and $L^2(\Omega)$ norms when h and ϵ are of the same order. To reduce the resonance effect caused by the boundary layer thickness of order $O(\epsilon)$, Hou and Wu [15] introduce an over-sampling technique which constructs the basis functions on a sampling element of size greater than $h + \epsilon$. For a detailed discussion of the multiscale FE method, we refer the reader to [15,16].

2.4. Computational cost

We comment on the computational cost of the multiscale FE method (MsFEM) by Hou et al. [15,16] in comparison with the standard FE method using linear basis functions (LFEM). Our remark also applies to other methods such as the multiscale FE method of Allaire and Brizzi [3] and the multiscale finite volume method [17], since these methods have a similar cost as MsFEM.

To facilitate the discussion, we assume that $\Omega = [0,1]^{d=2}$ and that the domain is decomposed into linear rectangular elements. We denote by L the number of intervals in the x- and y-directions. The total number of elements at the coarse grid level is thus $K = L \times L$. To compute the basis functions, each element Ω^k is divided into $M \times M$ subcell elements. Thus, the mesh size is $h = 1/L$ for the global problem (15) and is $H = h/M$ for the cell problems (13). The total number of elements at the fine grid level is $LM \times LM$. Note that the number of degrees of freedom is in the same order as the number of elements.

To make a fair assessment, we consider two distinct cases: (i) solving the original problem (1) for n_s different source terms and boundary conditions, and (ii) solving the problem (1) for n_m different media. We show the computational cost of LFEM and MsFEM in terms of both memory requirement and CPU time in Table 1 for Case (i) and in Table 2 for Case (ii). It is assumed that the computational cost of both methods scales linearly with n_s and n_m. The exact value of the constant γ depends on the solver used and on the sparsity of the stiffness matrix. For instance, in the case of LFEM, sparse–matrix iterative solvers typically incur $O(\mathcal{N})$ cost per iteration, and the number of iterations itself depend on the condition number of the matrix.

It is clear that MsFEM significantly reduces computer memory in both cases. Hence, MsFEM can solve much larger problems than LFEM. As regards the CPU time, in Case (i), the operation count is $O((LM)^{\gamma d})$ for LFEM and $O(n_e L^d M^{\gamma d} + n_s L^{\gamma d})$ for MsFEM. Note that MsFEM requires $O(n_e L^d M^{\gamma d})$ for pre-computing the bases and the stiffness matrix, then all the subsequent calculations take only $O(n_s L^{\gamma d})$ since we no longer need to compute the bases and the stiffness matrix. Therefore, MsFEM proves quite efficient for problems with multiple source terms and boundary conditions and the efficiency gain increases with n_s. However, in Case (ii), MsFEM is as computationally expensive as LFEM, because the bases and stiffness matrix have to be constructed anyway for each new medium.

3. Multiscale reduced-basis method

In this section, we consider solving parametrized elliptic PDEs with multiple scales by means of model reduction. First we continue Section 2.3 to introduce the multiscale FE approximation upon which our multiscale reduced basis approximation is built. We then discuss the development of the multiscale reduced basis method (MsRBM) and associated *a prior* convergence analysis. Finally, we describe the detailed implementation and analyze the computational cost.

3.1. Multiscale finite element approximation

Let $\varphi^{ki} \in H^1(\Omega^k)$ be functions satisfying the boundary conditions in (13). The solutions of the cell problems (13) can be found as

$$\phi^{ki}(\boldsymbol{\mu}) = \psi^{ki}(\boldsymbol{\mu}) + \varphi^{ki}, \quad 1 \leqslant k \leqslant K, 1 \leqslant i \leqslant n_e, \tag{18}$$

where $\psi^{ki}(\boldsymbol{\mu}) \in H_0^1(\Omega^k)$ is the solution of

$$a^k(\psi^{ki}(\boldsymbol{\mu}), v; \boldsymbol{\mu}) = f^{ki}(v; \boldsymbol{\mu}), \quad \forall v \in H_0^1(\Omega^k). \tag{19}$$

Here the forms are given by

$$\begin{aligned} a^k(w, v; \boldsymbol{\mu}) &= \int_{\Omega^k} g(\boldsymbol{x}; \boldsymbol{\mu}) \nabla w \cdot \nabla v \, d\boldsymbol{x}, \quad 1 \leqslant k \leqslant K, \\ f^{ki}(v; \boldsymbol{\mu}) &= -\int_{\Omega^k} g(\boldsymbol{x}; \boldsymbol{\mu}) \nabla \varphi^{ki} \cdot \nabla v \, d\boldsymbol{x}, \quad 1 \leqslant k \leqslant K, 1 \leqslant i \leqslant n_e. \end{aligned} \tag{20}$$

Note that the bilinear forms $a^k, 1 \leqslant k \leqslant K$, are symmetric positive-definite.

In each element Ω^k, we consider a triangulation, $\mathcal{T}_k$, which consists of non-overlapping elements with diameter $\leqslant H$ such that $\overline{\Omega}^k = \bigcup_{T \in \mathcal{T}_k} \overline{T}$. We introduce the FE approximation spaces

Table 1
Comparison between LFEM and MsFEM: memory requirement and CPU time for solving the problem (1) for different source terms and boundary conditions

Cost	LFEM	MsFEM
Memory	$O(L^d M^d)$	$O(L^d + M^d)$
CPU time	$O(n_s (LM)^{\gamma d})$	$O(n_e L^d M^{\gamma d} + n_s L^{\gamma d})$

Table 2
Comparison between LFEM and MsFEM: memory requirement and CPU time for solving the problem (1) for different media

Cost	LFEM	MsFEM
Memory	$O((LM)^d)$	$O(L^d + M^d)$
CPU time	$O(n_m (LM)^{\gamma d})$	$O(n_m (L^{\gamma d} + n_e L^d M^{\gamma d}))$

$$W_H^k = \{v \in H_0^1(\Omega^k) | v|_T \in \mathbb{P}_1(T),\ \forall T \in \mathcal{T}_k\}, \quad 1 \leqslant k \leqslant K, \tag{21}$$

where $\mathbb{P}_1(T)$ denotes the space of linear polynomials over T. The FE approximation $\psi_H^{ki}(\boldsymbol{\mu}) \in W_H^k$ is then found as

$$a^k(\psi_H^{ki}(\boldsymbol{\mu}), v; \boldsymbol{\mu}) = f^{ki}(v; \boldsymbol{\mu}), \quad \forall v \in W_H^k. \tag{22}$$

We define an associated FE approximation space as

$$Y_h(\boldsymbol{\mu}) = \text{span}\{\phi_H^{ki}(\boldsymbol{\mu}) : 1 \leqslant k \leqslant K, 1 \leqslant i \leqslant n_e\}. \tag{23}$$

Here $\phi_H^{ki}(\boldsymbol{\mu}) = \psi_H^{ki}(\boldsymbol{\mu}) + \varphi_H^{ki}$, where $\varphi_H^{ki} \in W_H^k$ is just the $L^2(\Omega)$ projection of φ^{ki} onto W_H^k.

Finally, the multiscale FE method seeks $u_h^Y \in Y_h(\boldsymbol{\mu})$ such that

$$a(u_h^Y(\boldsymbol{\mu}), v; \boldsymbol{\mu}) = \ell(v), \quad \forall v \in Y_h(\boldsymbol{\mu}). \tag{24}$$

The convergence properties of u_h^Y have been discussed in Section 2.3. In the next section, we describe the multiscale reduced basis method.

3.2. Multiscale reduced-basis approximation

As the point of departure for our development of MsRBM we assume that we are given K samples $S_J^k = \{\boldsymbol{\mu}^{kj} \in \mathcal{D}, 1 \leqslant j \leqslant J\}$, $1 \leqslant k \leqslant K$ of J parameter values and associated snapshot sets $\{\psi_H^{ki}(\boldsymbol{\mu}^{kj}), 1 \leqslant i \leqslant n_e\}_{j=1}^J$, $1 \leqslant k \leqslant K$, where $\psi_H^{ki}(\boldsymbol{\mu}^{kj})$ is the solution of (22) for $\boldsymbol{\mu} = \boldsymbol{\mu}^{kj}$. Next, for each k, we apply the proper orthogonal decomposition (POD) [19,31] to compute the basis set $\{\zeta_n^k, 1 \leqslant n \leqslant N_{\max}\}$ from the snapshot set $\{\psi_H^{ki}(\boldsymbol{\mu}^{kj}), 1 \leqslant i \leqslant n_e, 1 \leqslant j \leqslant J\}$, where we note that $N_{\max} = n_e J$. The POD method is well known and given in Appendix for reference. We then define our nested RB spaces as

$$W_N^k = \text{span}\{\zeta_n^k, 1 \leqslant n \leqslant N\}, \quad 1 \leqslant N \leqslant N_{\max}. \tag{25}$$

In general, the construction of our nested RB spaces W_N^k, amounts to compute $N_{\max}K$ solutions of (22) at the fine local mesh. However, for certain problems in which the parametrized function $g(\boldsymbol{x}; \boldsymbol{\mu})$ has a similar form on all elements Ω^k, we need only to compute $N_{\max}$ solutions. We shall return to this point when we discuss the computational cost in Section 3.4 and the numerical results in Section 4.

In order to solve the parametrized multiscale elliptic problem (1) for any given $\boldsymbol{\mu}$, we proceed as follows. First, we determine the RB approximations $\psi_N^{ki}(\boldsymbol{\mu}) \in W_N^k$ to $\psi_h^{ki}(\boldsymbol{\mu}) \in W_H^k$ from

$$a^k(\psi_N^{ki}(\boldsymbol{\mu}), v; \boldsymbol{\mu}) = f^{ki}(v; \boldsymbol{\mu}), \quad \forall v \in W_N^k, 1 \leqslant k \leqslant K, 1 \leqslant i \leqslant n_e. \tag{26}$$

This is essentially a Galerkin projection of (19) onto the RB space W_N^k. We then define our global FE approximation space as

$$Z_h(\boldsymbol{\mu}) = \text{span}\{\psi_N^{ki}(\boldsymbol{\mu}) + \varphi_H^{ki} : 1 \leqslant k \leqslant K, 1 \leqslant i \leqslant n_e\}. \tag{27}$$

Of course, $Z_h(\boldsymbol{\mu})$ has the same dimension as $Y_h(\boldsymbol{\mu})$. Finally, the multiscale RB method seeks $u_h^Z(\boldsymbol{\mu}) \in Z_h(\boldsymbol{\mu})$ such that

$$a(u_h^Z(\boldsymbol{\mu}), v; \boldsymbol{\mu}) = \ell(v; \boldsymbol{\mu}), \quad \forall v \in Z_h(\boldsymbol{\mu}). \tag{28}$$

Clearly, $u_h^Z(\boldsymbol{\mu})$ is an approximation to $u_h^Y(\boldsymbol{\mu})$ since $\psi_N^{ki}(\boldsymbol{\mu})$ is nothing but the RB approximation of $\psi_H^{ki}(\boldsymbol{\mu})$.

Some remarks about MsRBM are in order. First, the main difference between MsRBM and MsFEM lies in the approximation spaces used for the cell problems. Here the RB spaces span pre-computed solutions of the underlying equation at some parameter points. Owing to this property, $\psi_N^{ki}(\boldsymbol{\mu})$ converge rapidly to $\psi_H^{ki}(\boldsymbol{\mu})$ as the RB dimension N increases. In fact, *exponential* convergence of the RB error with respect to N can be proven for a simple one-parameter case [20]. As a result, N is typically chosen very small to achieve the desired accuracy. Second, as demonstrated in [26,29], the RB convergence rate does not depend on the dimension of the FE space W_H^k. This means that we can choose this dimension "arbitrarily" large to increase the accuracy at no detriment to (online) performance. Third, suppose that the space $Z_h(\boldsymbol{\mu}_{\text{old}})$ is already constructed for some $\boldsymbol{\mu}_{\text{old}}$ and that later we want to solve the problem for $\boldsymbol{\mu} = \boldsymbol{\mu}_{\text{new}}$ whereby $g(\boldsymbol{x}; \boldsymbol{\mu}_{\text{old}})$ and $g(\boldsymbol{x}; \boldsymbol{\mu}_{\text{new}})$ only differ in Ω^k, then we solve (26) for this particular element to update $Z_h(\boldsymbol{\mu}_{\text{new}})$. Of course, MsFEM can also update $Y_h(\boldsymbol{\mu}_{\text{new}})$ in the same way. This renders both MsRBM and MsFEM efficient for problems whereby the differential coefficient varies only in a local small region of the physical domain, since in this case we only need to recompute the reduced basis for the cell problems in the local region.

Fourth, and finally, as it is well known for coercive elliptic problems [25,30] that we can develop *a posteriori* error estimator $\Delta_N^{ki}(\boldsymbol{\mu})$ such that

$$\|\psi_N^{ki}(\boldsymbol{\mu}) - \psi_H^{ki}(\boldsymbol{\mu})\|_{W_H^k} \leqslant \Delta_N^{ki}(\boldsymbol{\mu}), \quad \forall \boldsymbol{\mu} \in \mathcal{D}. \tag{29}$$

where

$$\Delta_N^{ki}(\boldsymbol{\mu}) = \frac{1}{\hat{\alpha}^k(\boldsymbol{\mu})} \sup_{v \in W_H^k} \frac{r^{ki}(v; \boldsymbol{\mu})}{\|v\|_{W_H^k}}. \tag{30}$$

Here $\hat{\alpha}^k(\boldsymbol{\mu})$ is the lower bound of the coercivity constant $\alpha^k(\boldsymbol{\mu})$ defined as

$$\alpha^k(\boldsymbol{\mu}) = \inf_{v \in W_H^k} \frac{a^k(v,v;\boldsymbol{\mu})}{\|v\|^2_{W_H^k}}, \quad \beta^k(\boldsymbol{\mu}) = \sup_{v \in W_H^k} \frac{a^k(v,v;\boldsymbol{\mu})}{\|v\|^2_{W_H^k}}; \tag{31}$$

and $r^{ki}(v;\boldsymbol{\mu})$ is the residual given by

$$r^{ki}(v;\boldsymbol{\mu}) = f^{ki}(v;\boldsymbol{\mu}) - a^k(\psi_N^{ki}(\boldsymbol{\mu}), v;\boldsymbol{\mu}), \quad \forall v \in W_H^k. \tag{32}$$

It can be easily shown that

$$1 \leqslant \frac{\Delta_N^{ki}(\boldsymbol{\mu})}{\|\psi_N^{ki}(\boldsymbol{\mu}) - \psi_H^{ki}(\boldsymbol{\mu})\|_{W_H^k}} \leqslant \sqrt{\frac{\beta^k(\boldsymbol{\mu})}{\hat{\alpha}^k(\boldsymbol{\mu})}}, \quad \forall N \geqslant 1, \ \forall \boldsymbol{\mu} \in \mathcal{D}. \tag{33}$$

Hence, the error estimator is sharp and rigorous for the true error, and thus important for certification of the RB approximation.

Moreover, the error bound can also play an important role in adaptive sampling procedures to *optimally* select the sample points $S_J^k = \{\boldsymbol{\mu}^{kj} \in \mathcal{D}, 1 \leqslant j \leqslant J\}$ as we briefly describe: given a (random or deterministic) parameter point $S_1^k = \{\boldsymbol{\mu}^{k1}\}$, we compute $W_N^k = \text{span}\{\psi_H^{ki}(\boldsymbol{\mu}^{k1}), 1 \leqslant i \leqslant n_e\}$; for $j = 2, \ldots, J$, we find $\boldsymbol{\mu}^{kj} = \arg\max_{\mu \in \mathcal{D}} \max_{1 \leqslant i \leqslant n_e} \Delta_{N-1}^{ki}(\boldsymbol{\mu})$, set $S_j^k = S_{j-1}^k \cup \boldsymbol{\mu}^{kj}$, and update $W_N^k = W_{N-1}^k + \text{span}\{\psi_H^{ki}(\boldsymbol{\mu}^{kj}), 1 \leqslant i \leqslant n_e\}$. In essence, we find and include the parameter points which maximize the error bounds. The well-selected sample set will in turn ensure rapidly convergent and well-conditioned RB systems. Note that in the course of pursuing the greedy sampling procedure, we work with the hierarchical Lagrange basis and only apply POD on the Lagrange basis to obtain the POD basis at the end of the procedure. The justification for using the POD basis is that most energy/information of the Lagrange basis is captured in a number of leading POD basis functions, which may then lead to an improved reduced order model. Further details on the *a posteriori* error estimation and adaptive sampling procedure can be found in [24].

3.3. A priori convergence and error estimates

The *a priori* convergence of Galerkin approximations for coercive elliptic equations is classical. In fact, it is standard to demonstrate optimality of $\psi_N^{ki}(\boldsymbol{\mu})$ in the sense that

$$\|\psi_H^{ki}(\boldsymbol{\mu}) - \psi_N^{ki}(\boldsymbol{\mu})\|_{W_H^k} \leqslant \sqrt{\frac{\beta^k(\boldsymbol{\mu})}{\alpha^k(\boldsymbol{\mu})}} \inf_{v_N \in W_N^{ki}} \|\psi_H^{ki}(\boldsymbol{\mu}) - v_N\|_{W_H^k}. \tag{34}$$

This statement demonstrates the convergence of $\psi_N^{ki}(\boldsymbol{\mu}) \to \psi_H^{ki}(\boldsymbol{\mu})$ in the limit $W_N^k \to W_H^k$. It follows that for any $\varepsilon > 0$, there exists an integer $N(\varepsilon)$ such that

$$\|\psi_H^{ki}(\boldsymbol{\mu}) - \psi_N^{ki}(\boldsymbol{\mu})\|_{W_H^k} \leqslant \varepsilon, \quad \forall N \geqslant N(\varepsilon), \ \forall \boldsymbol{\mu} \in \mathcal{D}. \tag{35}$$

In practice, as mentioned earlier, $\psi_N^{ki}(\boldsymbol{\mu})$ converges very rapidly to $\psi_H^{ki}(\boldsymbol{\mu})$ with N. Exponential convergence can be theoretically shown for one-parameter model problem [20] and typically observed for multi-parameter problems [29].

The rapid convergence of RB approximations is important since it allows us to obtain the *a priori* error estimates for the RB solution u_h^Z as obtained for the multiscale FE solution u_h^Y. Let us formally put the result in the following lemma:

Lemma 1. *Let $u(\boldsymbol{\mu})$ be the solution of (1) and $u_h^Z(\boldsymbol{\mu})$ be its approximation computed by using MsRBM. Assuming that $\|\psi_N^{ki}(\boldsymbol{\mu}) - \psi_H^{ki}(\boldsymbol{\mu})\|_{W_H^k} \to 0$ for all $\boldsymbol{\mu} \in \mathcal{D}$ for $1 \leqslant k \leqslant K$ and $1 \leqslant i \leqslant n_e$. Then there exist positive constants C_1 and C_2, independent of ϵ and h, such that*

$$\|u(\boldsymbol{\mu}) - u_h^Z(\boldsymbol{\mu})\|_1 \leqslant C_1 h \|f\|_0 + C_2(\epsilon/h)^{\frac{1}{2}} \quad (\epsilon < h), \tag{36}$$

and, moreover,

$$\|u(\boldsymbol{\mu}) - u_h^Z(\boldsymbol{\mu})\|_0 = O(h^2 + \epsilon/h) \quad (\epsilon < h). \tag{37}$$

3.4. Numerical implementation

In this section, we develop the offline–online computational procedure [25,27,30] that allows us to efficiently compute $u_h^Z(\boldsymbol{\mu})$. We consider here elliptic problems with *affine parameter dependence*. Let $g^k(\boldsymbol{x};\boldsymbol{\mu})$ be the restriction of $g(\boldsymbol{x};\boldsymbol{\mu})$ on the element Ω^k. We suppose that for some finite (preferably small) integer Q^k, g^k may be expressed as

$$g^k(\boldsymbol{x};\boldsymbol{\mu}) = \sum_{q=1}^{Q^k} \Theta_q^k(\boldsymbol{\mu}) G_q^k(\boldsymbol{x}), \tag{38}$$

where for $q = 1, \ldots, Q^k$, $\Theta_q^k(\boldsymbol{\mu})$ depends only on $\boldsymbol{\mu}$ and $G_q^k(\boldsymbol{x})$ depends only on $\boldsymbol{x}$. Then the bilinear forms and linear functionals defined in (20) can be written as

$$
\begin{aligned}
a^k(w,v;\boldsymbol{\mu}) &= \sum_{q=1}^{Q^k} \Theta_q^k(\boldsymbol{\mu}) a_q^k(w,v), \quad 1 \leqslant k \leqslant K, \\
f^{ki}(v;\boldsymbol{\mu}) &= \sum_{q=1}^{Q^k} \Theta_q^k(\boldsymbol{\mu}) f_q^{ki}(v), \quad 1 \leqslant k \leqslant K, 1 \leqslant i \leqslant n_e,
\end{aligned}
\tag{39}
$$

where

$$
\begin{aligned}
a_q^k(w,v) &= \int_{\Omega^k} G_q^k(\boldsymbol{x}) \nabla w \cdot \nabla v \, d\boldsymbol{x}, \quad 1 \leqslant q \leqslant Q^k, \\
f_q^{ki}(v) &= -\int_{\Omega^k} G_q^k(\boldsymbol{x}) \nabla \varphi^{ki} \cdot \nabla v \, d\boldsymbol{x}, \quad 1 \leqslant r \leqslant Q^k.
\end{aligned}
\tag{40}
$$

It is important to note that the a_q^k and f_q^{ki} are *independent* of $\boldsymbol{\mu}$. The MsRBM method can be easily extended to treat *nonaffine parameter dependence*; see [4,24] for a detailed discussion.

We now describe the computational procedure. Since $\psi_N^{ki}(\boldsymbol{\mu}) \in W_N^k = \text{span}\{\zeta_n^k, 1 \leqslant n \leqslant N\}$, we expand it as

$$
\psi_N^{ki}(\boldsymbol{\mu}) = \sum_{n=1}^{N} c_n^{ki}(\boldsymbol{\mu}) \zeta_n^k,
\tag{41}
$$

where $c_n^{ki}(\boldsymbol{\mu})$, $1 \leqslant n \leqslant N$, are RB coefficients which must be determined. We then choose for test functions $v = \zeta_m^k$, $1 \leqslant m \leqslant N$, and insert (41) into (26) to arrive at the desired linear system for $\underline{c}^{ki}(\boldsymbol{\mu}) = [c_1^{ki}(\boldsymbol{\mu}), c_2^{ki}(\boldsymbol{\mu}), \ldots, c_N^{ki}(\boldsymbol{\mu})]^T \in \mathbb{R}^N$ as

$$
\underline{A}^k(\boldsymbol{\mu}) \underline{c}^{ki}(\boldsymbol{\mu}) = \underline{F}^{ki}(\boldsymbol{\mu}).
\tag{42}
$$

Here $\underline{A}^k(\boldsymbol{\mu}) \in \mathbb{R}^{N \times N}$ is a SPD matrix with entries $A_{mn}^k(\boldsymbol{\mu}) = a^k(\zeta_n^k, \zeta_m^k; \boldsymbol{\mu})$, $1 \leqslant n, m \leqslant N$, and $\underline{F}^{ki}(\boldsymbol{\mu}) \in \mathbb{R}^N$ is the vector with entries $F_n^{ki}(\boldsymbol{\mu}) = f^{ki}(\zeta_n^k; \boldsymbol{\mu})$, $1 \leqslant n \leqslant N$. Since $\underline{A}^k(\boldsymbol{\mu})$ is full, inverting it will take $O(N^3)$ operations and the multiplication of the inverse of $\underline{A}^k(\boldsymbol{\mu})$ with $\underline{F}^{ki}(\boldsymbol{\mu})$, $1 \leqslant i \leqslant n_e$, takes $O(n_e N^2)$. Therefore, the computation of $\underline{c}^{ki}(\boldsymbol{\mu})$, $1 \leqslant i \leqslant n_e$, takes $O(N^3 + n_e N^2)$ operations.

Next, we invoke the affine decomposition (39) and (40) to write

$$
\begin{aligned}
\underline{A}^k(\boldsymbol{\mu}) &= \sum_{q=1}^{Q^k} \Theta_q^k(\boldsymbol{\mu}) \underline{A}_q^k, \\
\underline{F}^{ki}(\boldsymbol{\mu}) &= \sum_{q=1}^{Q^k} \Theta_q^k(\boldsymbol{\mu}) \underline{F}_q^{ki},
\end{aligned}
\tag{43}
$$

where $\underline{A}_q^k \in \mathbb{R}^{N \times N}$, $1 \leqslant q \leqslant Q^k$, and $\underline{F}_q^{ki} \in \mathbb{R}^N$, $1 \leqslant q \leqslant Q^k$, are given by

$$
\begin{aligned}
A_{q\,mn}^k &= a_q^k(\zeta_n^k, \zeta_m^k), \quad 1 \leqslant n, m \leqslant N, \\
F_{q\,n}^{ki} &= f_q^{ki}(\zeta_n^k), \quad 1 \leqslant n \leqslant N.
\end{aligned}
\tag{44}
$$

We note that these quantities do not depend on $\boldsymbol{\mu}$ and can therefore be pre-computed offline.

It remains to assemble the global stiffness matrix and right hand side for (28). To this end, we note that on each element Ω^k the elemental matrix $\underline{E}^k(\boldsymbol{\mu}) \in \mathbb{R}^{n_e \times n_e}$ and vector $\underline{e}^k(\boldsymbol{\mu}) \in \mathbb{R}^{n_e}$ have entries

$$
E_{ij}^k(\boldsymbol{\mu}) = \int_{\Omega^k} g^k(\boldsymbol{x}; \boldsymbol{\mu}) \nabla \left(\psi_N^{ki}(\boldsymbol{\mu}) + \varphi_H^{ki} \right) \cdot \nabla \left(\psi_N^{kj}(\boldsymbol{\mu}) + \varphi_H^{kj} \right) d\boldsymbol{x}, \quad e_i^k(\boldsymbol{\mu}) = \int_{\Omega^k} f(\boldsymbol{x}) \left(\psi_N^{ki}(\boldsymbol{\mu}) + \varphi_H^{ki} \right) d\boldsymbol{x},
\tag{45}
$$

for $1 \leqslant i, j \leqslant n_e$. Inserting (38) and (41) into (45) and noting from (40), we obtain

$$
E_{ij}^k(\boldsymbol{\mu}) = \sum_{q=1}^{Q^k} \Theta_q^k(\boldsymbol{\mu}) \left(\underline{c}^{ki}(\boldsymbol{\mu})^T \underline{A}_q^k \underline{c}^{kj}(\boldsymbol{\mu}) + 2 \underline{c}^{ki}(\boldsymbol{\mu})^T \underline{B}_q^{kj} + \underline{C}_q^{kij} \right), \quad e_i^k(\boldsymbol{\mu}) = \underline{c}^{ki}(\boldsymbol{\mu})^T \underline{L}^k + \underline{D}^{ki},
\tag{46}
$$

where for $1 \leqslant k \leqslant K$, $1 \leqslant i, j \leqslant n_e$, $1 \leqslant q \leqslant Q^k$, $\underline{B}_q^{ki} \in \mathbb{R}^N$, $\underline{L}^k \in \mathbb{R}^N$, $\underline{C}_q^{kij} \in \mathbb{R}$, and $\underline{D}^{ki} \in \mathbb{R}$ have entries

$$
\begin{aligned}
B_{qn}^{ki} &= \int_{\Omega^k} G_q^k(\boldsymbol{x}) \nabla \zeta_n^k \cdot \nabla \varphi_H^{ki} d\boldsymbol{x}, \quad 1 \leqslant n \leqslant N, \\
L_n^k &= \int_{\Omega^k} f(\boldsymbol{x}) \zeta_n^k d\boldsymbol{x}, \quad 1 \leqslant n \leqslant N, \\
C_q^{kij} &= \int_{\Omega^k} G_q^k(\boldsymbol{x}) \nabla \varphi_H^{ki} \cdot \nabla \varphi_H^{kj} d\boldsymbol{x}, \\
D^{ki} &= \int_{\Omega^k} f(\boldsymbol{x}) \varphi_H^{ki} d\boldsymbol{x}.
\end{aligned}
\tag{47}
$$

Finally, we assemble the elemental matrices $\underline{E}^k(\boldsymbol{\mu})$ and vectors $\underline{e}^k(\boldsymbol{\mu})$, $1 \leqslant k \leqslant K$, to form the algebraic system of equations associated with (28). We summarize the computational process in Table 3.

The operation count of the offline stage includes the computational cost of the adaptive sampling procedure outlined in Section 3.2, $N_{\max}K$ solves of (22), the POD procedure for K snapshot sets of size $N_{\max}$, and $O(KQN_{\max}^2)$ inner products. Here Q is the maximum of $Q^k, 1 \leqslant k \leqslant K$. The offline stage is thus computationally intensive, but performed only once. However, for problems in which Ω^k and $g^k(\boldsymbol{x};\boldsymbol{\mu})$, $1 \leqslant k \leqslant K$, are all the same, we only compute the offline quantities for any particular element and apply the results to other elements. As a result, the offline cost is reduced by a factor of K in such case.

The operation count of the online stage includes $O(K(QN^2 + n_eQN))$ to form $\underline{A}^k(\boldsymbol{\mu})$ and $\underline{F}^{ki}(\boldsymbol{\mu})$, $1 \leqslant k \leqslant K, 1 \leqslant i \leqslant n_e$, $O(K(N^3 + n_eN^2))$ to compute $\underline{c}_N^{ki}(\boldsymbol{\mu})$, $1 \leqslant k \leqslant K, 1 \leqslant i \leqslant n_e$, $O(KQN^2 + n_eKQN)$ to compute $\underline{E}^k(\boldsymbol{\mu})$ and $\underline{e}^k(\boldsymbol{\mu})$, $1 \leqslant k \leqslant K$, and $O((Kn_e)^\gamma))$ to solve the global linear system for $u_h^Z(\boldsymbol{\mu})$. The online complexity is thus $O(K(N^3 + n_eN^2 + QN^2 + n_eQN) + (Kn_e)^\gamma)$. The computer memory required is $O(N^3 + QN^2 + QN + Kn_e)$.

The crucial point is that once the offline stage is done, we can perform repetitive simulations of the underlying multiscale PDE for a wide variation of the differential coefficient with an affordable computational cost. To make the point more precise, we turn back to our discussion of the computational cost in Section 2.4. We assume that $\Omega = [0,1]^{d=2}$ and that the domain is decomposed into $L \times L$ linear rectangular elements. Each element is further divided into $M \times M$ subcell elements. We further assume that the Q is $O(1)$ and that $O(L^{\gamma d})$ is small relative to $O(n_eL^dM^{\gamma d})$. Then the computer memory and operation count for LFEM, MsFEM, and MsRBM are tabulated in Table 4. We note that while the memory requirement is similar, the ratio of the operation count between MsRBM and MsFEM is

$$\kappa_{\text{MsFEM/MsRBM}} = \frac{n_eM^{d\gamma}}{N^3}.$$

Therefore, MsRBM is efficient and thus relevant only when N^3 is small relative to $n_eM^{d\gamma}$.

4. Numerical application

4.1. Problem description

In this section, we apply the multiscale reduced-basis method to steady state single phase flows through random porous media of the form (1). We consider $\Omega = (0,1) \times (0,1)$, $u = 0$ on $\partial\Omega$, and $f = 1$. This is a model of flow in an oil reservoir with uniform injection into the domain and outflow at the boundaries. A uniform finite element mesh is constructed by decomposing Ω into $L \times L$ rectangular (actually square) elements. The number of cell problems is $K = L \times L$. The multiscale methods further subdivides each element into $M \times M$ subcell elements. We note that $h = 1/L$ and $H = 1/M$. For simplicity, linear boundary conditions are used in the cell problems. Reference solutions are computed on the well-resolved mesh of $LM \times LM$ elements using the linear finite element method.

The permeability field $g(\boldsymbol{x};\boldsymbol{\mu})$ is defined on a 72×72 grid over the domain Ω as shown in Fig. 1(a). For each grid cell, the value of g may vary randomly in the interval $[0.01, 1]$. The problem thus has $P = 72^2 = 5184$ parameters for the parametrization of the permeability field and $\boldsymbol{\mu} \in \mathcal{D} \equiv [0.01, 1]^P$. We fix $LM = 720$ which corresponds to 100 elements per parameter grid cell. This resolution is fine enough to serve as a reference. We consider $L = 18, 24, 36$, and 72. We note that the elements

Table 3
A flow chart for implementation of MsRBM

Offline stage
For each element $\Omega^k, 1 \leqslant k \leqslant K$, we do only once:
1. Perform the adaptive sampling procedure (see in Section 3.2) to compute the sample set $S_j^k = \{\boldsymbol{\mu}_j^k \in \mathcal{D}, 1 \leqslant j \leqslant J\}$
2. Solve the discrete cell problems (22) for $\{\psi_H^{ki}(\boldsymbol{\mu}_j^k), 1 \leqslant i \leqslant n_e, 1 \leqslant j \leqslant J\}$
3. Apply POD to compute $\{\zeta_n^k\}_{n=1}^{N_{\max}}$ from the above snapshot set
4. Compute and store $\underline{A}_q^k \in \mathbb{R}^{N\times N}$, $\underline{F}_q^{ki} \in \mathbb{R}^N$ from (44), $\underline{B}_q^{ki} \in \mathbb{R}^N$, $\underline{L}^k \in \mathbb{R}^N$, $C_q^{kij} \in \mathbb{R}$, and $\underline{D}^{ki} \in \mathbb{R}$ from (47) for $1 \leqslant i,j \leqslant n_e$, and $1 \leqslant q \leqslant Q$

Online stage
For each new $\boldsymbol{\mu} \in \mathcal{D}$, we compute $u_h^Z(\boldsymbol{\mu})$ as follows:
1. Assemble $\underline{A}^k(\boldsymbol{\mu}) \in \mathbb{R}^{N\times N}$ and $\underline{F}^{ki}(\boldsymbol{\mu}) \in \mathbb{R}^N$, $1 \leqslant k \leqslant K, 1 \leqslant i \leqslant n_e$, from (43)
2. Solve (42) for $\underline{c}^{ki}(\boldsymbol{\mu}) \in \mathbb{R}^N$, $1 \leqslant k \leqslant K, 1 \leqslant i \leqslant n_e$
3. Compute $\underline{E}^k(\boldsymbol{\mu}) \in \mathbb{R}^{n_e\times n_e}$ and $\underline{e}^k(\boldsymbol{\mu}) \in \mathbb{R}^{n_e}$, $1 \leqslant k \leqslant K$, from (46)
4. Form and solve the global linear system

Table 4
Comparison of LFEM, MsFEM,and MsRBM: memory requirement and CPU time to solve the parametrized problem (1) for different value of $\boldsymbol{\mu}$

Cost	LFEM	MsFEM	MsRBM
Memory	$O((LM)^d)$	$O(L^d + M^d)$	$O(N^3 + L^d)$
CPU time	$O((LM)^{\gamma d})$	$O(L^{\gamma d} + n_eL^dM^{\gamma d})$	$O(L^{\gamma d} + L^d(N^3 + (Q + n_e)N^2))$

$\Omega^k, 1 \leqslant k \leqslant K$, are identical and that the differential coefficient $g(\boldsymbol{x};\boldsymbol{\mu})$ has a similar form in all elements. Therefore, all the cell problems can now be recast in the reference element $\Omega_{\text{ref}} = [0,1/L] \times [0,1/L]$ which consists of $(72/L) \times (72/L)$ grid cells. Furthermore, these cell problems have $P_{\text{ref}} = (72/L) \times (72/L)$ parameters, $(\mu_1^k, \ldots, \mu_{P_{\text{ref}}}^k)$, which reside in a parameter space $\mathcal{D}_{\text{ref}} = [0.01,1]^{P_{\text{ref}}}$. In summary, each the cell problem has

$$\Theta_q^k = \mu_q^k, \quad G_q^k(\boldsymbol{x}) = \begin{cases} 1 & \text{if } \boldsymbol{x} \in \mathcal{R}_q, \\ 0 & \text{otherwise}, \end{cases} \tag{48}$$

where for $1 \leqslant q \leqslant Q_{\text{ref}} = P_{\text{ref}}$, $\mu_q^k \in [0.01,1]$ and $\mathcal{R}_q$ correspond to the regions associated with the respective cells as indicated in Fig. 1(b). Therefore, we need only to compute and store $\underline{A}_q^k \in \mathbb{R}^{N\times N}$, $\underline{B}_q^{ki} \in \mathbb{R}^N$, $\underline{L}_N^k \in \mathbb{R}^N$, $\underline{C}_q^{kij} \in \mathbb{R}$, $\underline{D}^{ki} \in \mathbb{R}$, and $\underline{F}_q^{ki} \in \mathbb{R}^N$, $1 \leqslant i,j \leqslant n_e$, $1 \leqslant r \leqslant Q_{\text{ref}}$ for the reference element Ω_{ref}. In this way, the computational cost of the offline stage is reduced by a factor of K.

We consider four different random realizations of the permeability field. The first realization g_1 is normal distribution with mean 0.5 and standard deviation 0.15. The second realization g_2 is log-normal distribution calculated from $0.025 \times 10^{1.6g_1}$. The third realization g_3 is independent and identically distributed (i.i.d) uniform distribution in the interval $[0.01,1]$. And the fourth realization g_4 is i.i.d normal distribution with mean 0.5 and standard deviation 0.15. These random fields are shown in Fig. 2. The first realization is generated using a spectral method [28]. At each spatial point in the 72×72 grid, the value of g_1 is given by the sum of 72 Fourier modes with low to high frequencies, which are uniformly distributed random phases in the interval $[0,2\pi]$. The shortest wavelength of this random field is thus $1/72$ and it is well resolved on the 720×720 grid since there are 11 nodes per shortest wavelength. However, the shortest wave length is not resolved on the $L \times L$ grid as we consider $L \leqslant 72$. The last two realizations are spatially uncorrelated uniform random field and Gaussian random field, respectively. We note that the four realizations of the permeability fields are stationary random fields and that the Gaussian random fields g_1 and g_4 are generated such that they take values in $[0.01,1.0]$.

Below we present numerical results obtained with using LFEM, MsFEM, and MsRBM. We assess the accuracy of the methods with the error measure

$$E_{\text{h}}(\boldsymbol{\mu}) = \frac{\|u_r(\boldsymbol{\mu}) - u_{\text{h}}(\boldsymbol{\mu})\|_{L^2(\Omega)}}{\|u_r(\boldsymbol{\mu})\|_{L^2(\Omega)}}. \tag{49}$$

Here the subscript r refers to the reference solution and the subscript h denotes computed solutions. All calculations are implemented and performed in Matlab® environment.

4.2. Numerical results

We first look at convergence of the RB approximation for the cell problems. To develop FE approximation for the cell problems, we use classical $\mathbb{P}1$ Lagrange finite elements on a quadrangular and uniform FE mesh shown in Fig. 1(c). The RB convergence is performed for a random sample Ξ^{test} of size $n^{\text{test}} = 1000$ over the parameter domain $\mathcal{D}_{\text{ref}}$. We define the maximum error as

$$\varepsilon_N^{\max} = \max_{1\leqslant i\leqslant n_e} \max_{\boldsymbol{\mu}_{\text{ref}}\in\Xi^{\text{test}}} \|\psi_H^i(\boldsymbol{\mu}_{\text{ref}}) - \psi_N^i(\boldsymbol{\mu}_{\text{ref}})\|_{H^1(\Omega_{\text{ref}})}. \tag{50}$$

Here $\psi_H^i(\boldsymbol{\mu}_{\text{ref}})$ and $\psi_N^i(\boldsymbol{\mu}_{\text{ref}})$, $1 \leqslant i \leqslant n_e$, are the FE solutions and RB solutions of the cell problems, respectively.

We present in Fig. 3(a) the maximum error, $\varepsilon_N^{\max}$, as a function of N for $L = 36$ corresponding to the parameter domain $\mathcal{D}_{\text{ref}}$ of $P_{\text{ref}} = 4$ parameters; Fig. 3(b) and (c) provide the same quantities for $L = 24$ ($P_{\text{ref}} = 9$) and $L = 18$ ($P_{\text{ref}} = 16$), respectively. We observe that the RB approximation converges very rapidly (exponentially with the RB dimension N). Note that the rate of

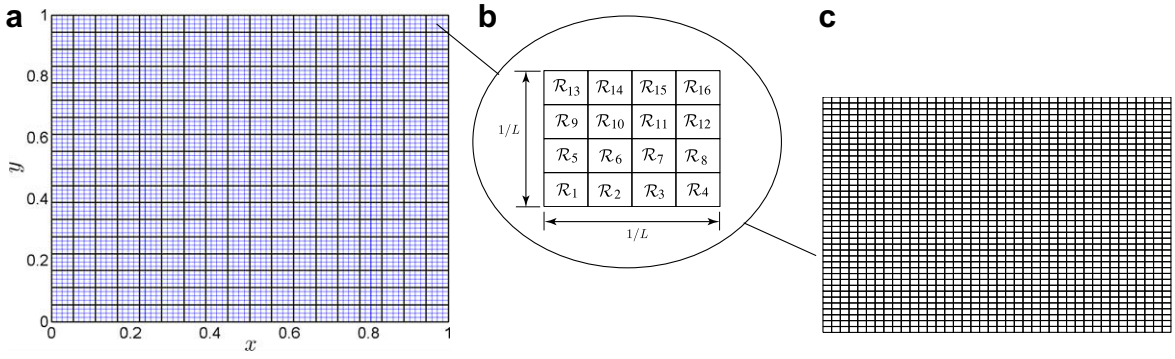

Fig. 1. The porous media flow problem: (a) permeability grid of 72×72 cells, (b) reference cell element $\Omega_{\text{ref}} = [0,1/L] \times [0,1/L]$ of $Q_L = (72/L) \times (72/L)$ cells (for $L = 18$), and (c) FE mesh on Ω_{ref}. Note that our cell problems are formulated on Ω_{ref} which depends on the upscaling dimension L.

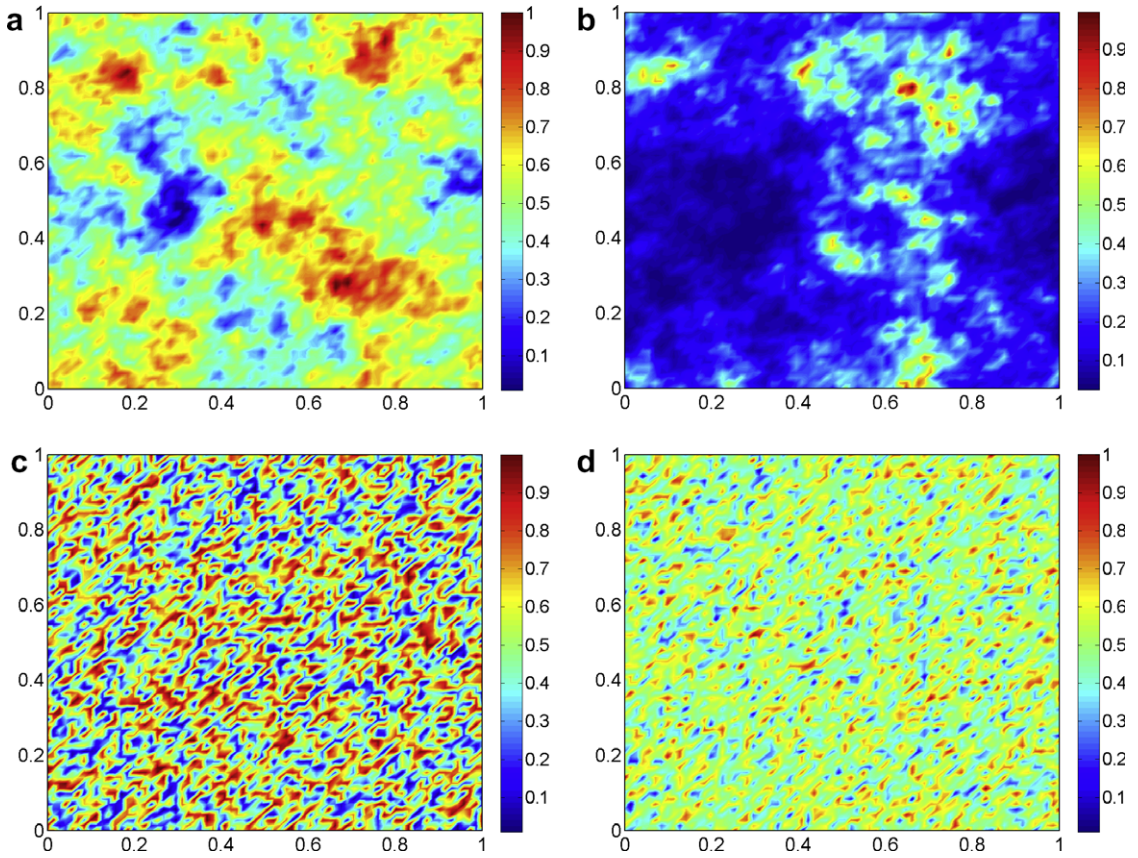

Fig. 2. Four different random realizations of the permeability field: (a) normal distribution, (b) log-normal distribution, (c) i.i.d uniform distribution, and (d) i.i.d. normal distribution. The first two realizations are generated using the spectral method.

convergence decreases with L since the number of parameters increases by a factor of 4 when we decrease L by a factor of 2. As a result, the number of snapshots and basis functions required to achieve the desired accuracy also increases as L decreases.

We next present in Table 5 the relative errors in $L^2(\Omega)$ norm obtained using the various methods for the normal distribution of the permeability shown in Fig. 2(a). We see that the errors decreases as L increases (h decreases). For small values of L such as $L = 18$ and $L = 24$, the errors of using the multiscale methods is almost one order of magnitude smaller than the error of using LFEM. We next give in Table 6 the results for the log-normal distribution of the permeability shown in Fig. 2(b). The results indicate the same trend of convergence observed in Table 5: the errors are reduced with increasing L.

We further present the errors in Table 7 for the i.i.d. uniform distribution of the permeability (in Fig. 2(c)) and in Table 8 for the i.i.d. normal distribution of the permeability (in Fig. 2(d)). We see that different from the two previous cases, the errors of using the multiscale methods initially increases as h decreases. This trend reverses when h becomes closer to the smallest scale of the problem. In the third case, the errors of using the multiscale methods have the same order of magnitude as the errors of using LFEM even when L is small. We note that the errors in the third case converge slower than those in the other cases. This is because the i.i.d uniform distribution yields more complex permeability field and solution structure than the other distributions.

In all four cases of the permeability field, we note that the differences in the errors of using MsFEM and MsRBM are very small, which implies that MsRBM has the same order of convergence as MsFEM. This is consistent with our a priori convergence result stated in Lemma 1.

We now study the convergence of the multiscale RB solution with respect to the RB dimension N. We present in Fig. 4 the relative errors obtained using MsRBM for the four realizations of the permeability. It is clear that the errors of using MsRBM decrease rapidly toward the errors of of using MsFEM as we increase N. For example, the combinations $(N, L) = (10, 36)$, $(N, L) = (30, 24)$, and $(N, L) = (50, 18)$ yield results which are quite close to those obtained using MsFEM as seen in Tables 5–8. Furthermore, we note that as L decreases MsRBM needs larger N in order to achieve a similar accuracy as MsFEM. This is due to the fact that the number of parameters for each cell problem is inversely proportional to $L \times L$ and that N required to satisfy the desired accuracy increases significantly as the number of parameters increases observed in Fig. 3. Therefore, L and N must be chosen on the basis of efficiency and accuracy of MsRBM. Since the computational cost of the online stage is

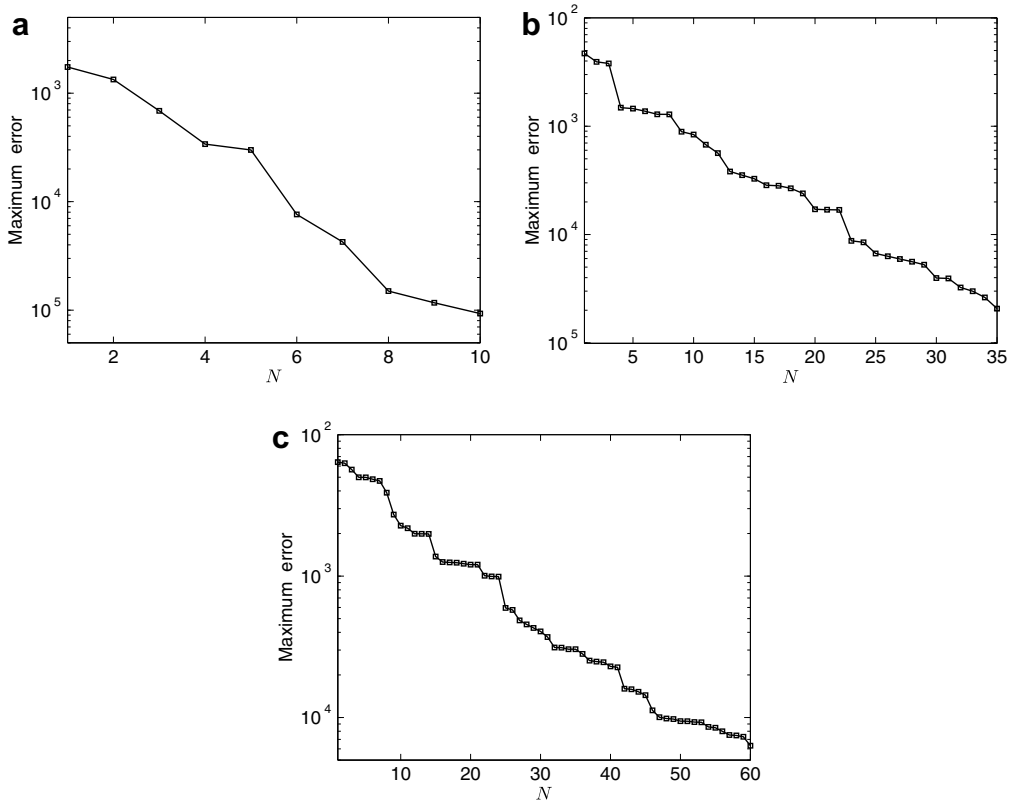

Fig. 3. The maximum error $\varepsilon_N^{\max}$ as a function of N for: (a) $L = 36$, (b) $L = 24$, and (c) $L = 18$.

Table 5
Relative errors in $L^2(\Omega)$ norm as a function of L for LFEM, as a function of L and M for MsFEM, and as a function of L and N for MsRBM for the 1st realization of the permeability field

L	M	N	LFEM	MsFEM	MsRBM
18	40	50	0.0304	0.0045	0.0045
24	30	30	0.0252	0.0038	0.0038
36	20	10	0.0102	0.0034	0.0034
72	10	1	0.0012	0.0012	0.0012

Table 6
Relative errors in $L^2(\Omega)$ norm as a function of L for LFEM, as a function of L and M for MsFEM, and as a function of L and N for MsRBM for the 2nd realization of the permeability field

L	M	N	LFEM	MsFEM	MsRBM
18	40	50	0.0405	0.0127	0.0129
24	30	30	0.0389	0.0115	0.0116
36	20	10	0.0130	0.0079	0.0079
72	10	1	0.0028	0.0028	0.0028

Table 7
Relative errors in $L^2(\Omega)$ norm as a function of L for LFEM, as a function of L and M for MsFEM, and as a function of L and N for MsRBM for the 3rd realization of the permeability field

L	M	N	LFEM	MsFEM	MsRBM
18	40	50	0.0773	0.0652	0.0687
24	30	30	0.1037	0.0743	0.0750
36	20	10	0.0622	0.0884	0.0884
72	10	1	0.0578	0.0578	0.0578

Table 8
Relative errors in $L^2(\Omega)$ norm as a function of L for LFEM, as a function of L and M for MsFEM, and as a function of L and N for MsRBM for the 4th realization of the permeability field

L	M	N	LFEM	MsFEM	MsRBM
18	40	50	0.0387	0.0109	0.0118
24	30	30	0.0278	0.0155	0.0157
36	20	10	0.0194	0.0184	0.0184
72	10	1	0.0123	0.0123	0.0123

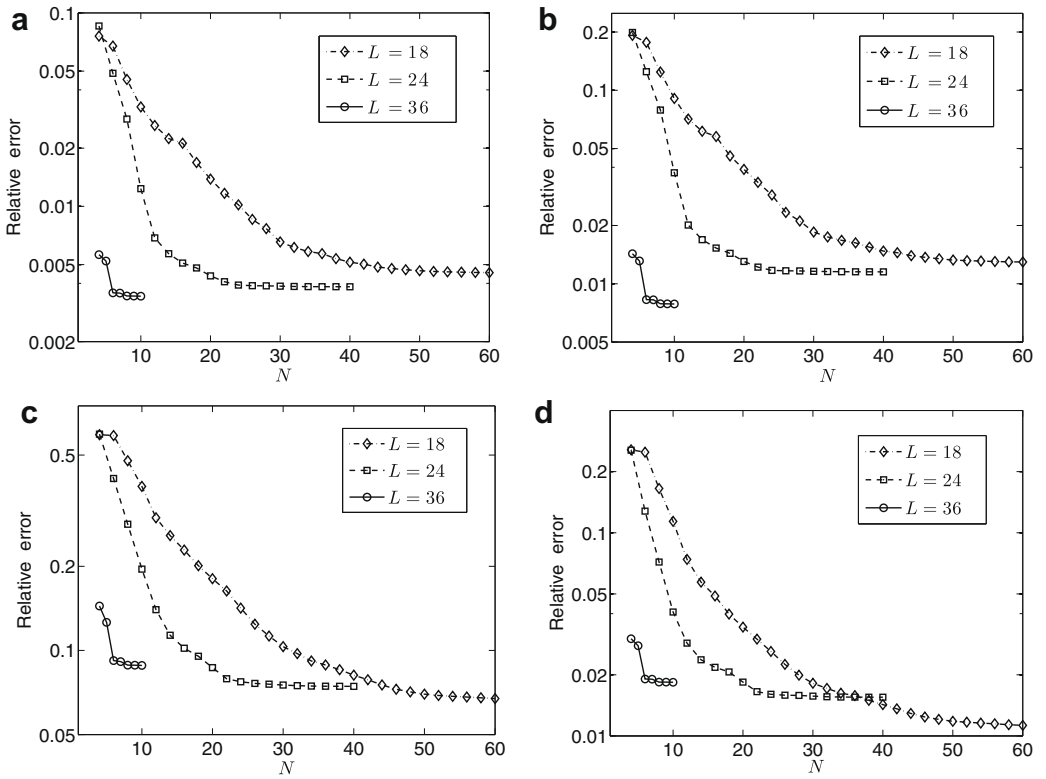

Fig. 4. Relative errors in $L^2(\Omega)$ norm (obtained using MsRBM) as a function of N for $L = 18, 24$ and 36 for: (a) normal distribution, (b) log-normal distribution, (c) i.i.d uniform distribution, and (d) i.i.d. normal distribution.

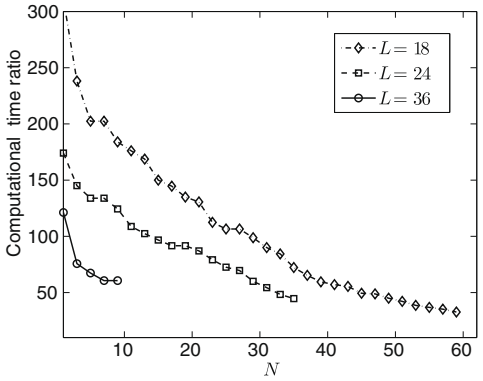

Fig. 5. The ratio of the computational times between MsFEM and MsRBM versus the RB dimension N for $L = 18, 24$ and 36.

$O(L^{\gamma d} + n_e L^d N^3)$, using smaller N and larger L is better than using larger N and smaller L for a given accuracy. So the pair $(N, L) = (10, 36)$ is more efficient than $(30, 24)$ and $(50, 18)$. This is in contrast to MsFEM which favors the smaller value of L.

Finally, we show in Fig. 5 the ratio of the computational times between MsFEM and MsRBM as a function of N for $L = 18, 24$ and 36. We see that the computational time ratio decreases with increasing N. Nevertheless, thanks to the rapid convergence of the RB approximation, MsRBM reduces computational time by a factor of 50, while providing a similar accuracy. The crucial new capability is fast RB calculations that permit us to efficiently treat a large number of cell problems at the fine local mesh, thereby providing rapid repeated solution of the elliptic problem for a wide range of porous media; for any given realization of the permeability field in the parameter space, the problem may be solved online within 7 seconds for $L = 18$ and $N = 50$, 4 seconds for $L = 24$ and $N = 30$, 3 seconds for $L = 36$ and $N = 10$, 9 seconds for $L = 72$ and $N = 1$ on a Pentium IV 1.73 GHz laptop. The computational efficiency renders MsRBM deemed useful for analysis of multiscale systems in composite materials and porous media.

5. Conclusions

We have presented a multiscale reduced-basis method for the efficient solution of multiscale parametrized elliptic PDEs. The problems have heterogeneous coefficients that are characterized by a very large number of independent parameters. Our approach involves the development of reduced order modeling for the homogeneous cell problems, since resolution of the cell problems is the most expensive operation in a multiscale method. To render the model reduction process efficient, we develop an offline–online computational procedure for the generation and simulation of a reduced order model. The offline stage is performed only one time, while the online stage can be repeated many times for any new medium. In addition, we exploit similarity of parametrization to replicate the reduced order model from one element to the other, thereby reducing the offline cost quite significantly. The operation count of the online stage depends on the cubic power of N – the dimension of the reduce order model. However, since the reduced basis spaces are constructed upon snapshots optimally selected by the adaptive sampling procedure, N is typically small. We have also shown that the method inherits the convergence properties of the multiscale FE method.

Numerical experiment confirms uniformly rapid convergence of the RB approximation and the error estimates in L^2 norm. Through comparison with the multiscale FE method we demonstrate that the proposed method reduces significantly the computational cost, while retaining the accuracy of the high-fidelity FE model. As a result, solution of the underlying PDE can be obtained rapidly and accurately for any given parameter value in the range considered. The method is thus relevant to parameter design and optimization in multiscale processes.

However, many questions remains as regards the extension of the multiscale RB method to treat parametrized multiscale problems more satisfactorily. In many cases, the oversampling technique can significantly improve the accuracy of the multiscale methods. Extension of this method to treat oversampling is thus necessary and subject to an ongoing investigation. Although we develop the *a posteriori* error bounds for the solution of the cell problems and use these error bounds in the adaptive sampling procedure, *a posteriori* error estimation for quantifying a multiscale RB approximation remains an open and challenging task. Another direction in future research is the extension of this work to explore how the accuracy of the RB approximation depends on the covariance structure of the permeability field and more generally to treat non-stationary random fields. Further developments are needed and may lead to a fast and reliable tool for solving parametrized PDEs with multiple scales, thereby enabling the reach of this method to important applications such as inverse problems.

Acknowledgments

I would like to thank Professor Yvon Maday of University of Paris VI, Professor A.T. Patera and Professor J. Paraire of MIT for many contributions to this work. I would also like to thank Dr. G. Rozza from MIT and Dr. D.B.P. Huynh from Northwestern University for fruitful discussions. Finally, I am thankful to the reviewers for their valuable comments that lead to a better presentation of this paper.

Appendix A. Proper orthogonal decomposition

The proper orthogonal decomposition (POD), also known as the Karhunen-Loève expansion, has found its applications in many areas of engineering disciplines such as pattern recognition, image processing, signal analysis, data compression, etc. [14]. The method has also been extensively used by the model reduction community to construct a set of basis functions which may significantly reduce the degrees of freedom required to fulfill a given error tolerance when they are used in place of the FE basis. Below we briefly describe the method and refer the reader to a wide body of literature [14,21,22,31] for a thorough discussion.

We aim to generate an optimal (in the mean square error sense) basis set $\{\zeta_n\}_{n=1}^N$ from any given (parameter-correlated) set of $N_{\max} (\geqslant N)$ snapshots $\{\xi_k\}_{k=1}^{N_{\max}}$. To this end, let $V_N = \text{span}\{v_1, \ldots, v_N\} \subset \text{span}\{\xi_1, \ldots, \xi_{N_{\max}}\}$ be an "arbitrary" space of dimension N. Without loss of generality, we assume that the space V_N is orthonormal such that $(v_n, v_m) = \delta_{nm}$, $1 \leqslant n, m \leqslant N$. (Note that $(\cdot, \cdot)$ denotes an appropriate inner product.) The POD space, $W_N = \text{span}\{\zeta_1, \ldots, \zeta_N\}$, is defined as

$$W_N = \arg \min_{V_N \subset \mathrm{span}\{\xi_1,\ldots,\xi_{N_{\max}}\}} \left(\frac{1}{N_{\max}} \sum_{k=1}^{N_{\max}} \inf_{\underline{\alpha}^k \in \mathbb{R}^N} \|\xi_k - \sum_{n=1}^{N} \alpha_n^k v_n\|^2 \right). \tag{A.1}$$

It follows from the orthornormality of V_N that $\alpha_n^k = (\xi_k, v_n), 1 \leqslant n \leqslant N, 1 \leqslant k \leqslant N_{\max}$. Hence, we have

$$W_N = \arg \min_{V_N \subset \mathrm{span}\{\xi_1,\ldots,\xi_{N_{\max}}\}} \left(\frac{1}{N_{\max}} \sum_{k=1}^{N_{\max}} \|\xi_k - \sum_{n=1}^{N} (\xi_k, v_n) v_n\|^2 \right). \tag{A.2}$$

We then expand the objective and invoke the orthornormality of the space V_N to arrive a maximization problem

$$W_N = \arg \max_{V_N \subset \mathrm{span}\{\xi_1,\ldots,\xi_{N_{\max}}\}} \frac{1}{N_{\max}} \sum_{k=1}^{N_{\max}} \sum_{n=1}^{N} (\xi_k, v_n)^2. \tag{A.3}$$

This maximization problem means to find the basis set W_N that captures the most energy possible. Hence, the error minimization notion of optimality is equivalent to the energy maximization notion of optimality, which is exactly the idea on which the Karhunen-Loève expansion is based.

In particular, we can construct the POD spaces by using the method of snapshots [31]. We first form the correlation matrix $\underline{C} \in \mathbb{R}^{N_{\max} \times N_{\max}}$ given by

$$C_{ij} = \frac{1}{N_{\max}} (\xi_i, \xi_j), \quad 1 \leqslant i,j \leqslant N_{\max}. \tag{A.4}$$

We then look for the eigenpairs ($\underline{\chi}^k \in \mathbb{R}^{N_{\max}}, \lambda^k \in \mathbb{R}_{+0}$) satisfying

$$\underline{C}\underline{\chi}^k = \lambda^k \underline{\chi}^k. \tag{A.5}$$

Note that the eigenvalues are arranged in descending order $\lambda_1 \geqslant \lambda_2 \geqslant \cdots \geqslant \lambda_{N_{\max}}$. We finally compute the basis functions ζ_n as

$$\zeta_n = \sum_{k=1}^{N_{\max}} \chi_k^n \xi_k, \quad 1 \leqslant n \leqslant N. \tag{A.6}$$

Here the eigenvector $\underline{\chi}^n$ corresponds to the eigenvalue λ^n.

From the above construction it should be clear that POD spaces are not only optimal and orthonormal, but also hierarchical – $W_1 \subset W_2 \subset \cdots \subset W_N$. The POD can also work in other Banach spaces such as $L^2(\Omega)$.

References

[1] J. Aarnes, B.O. Heimsun, Multiscale discontinuous Galerkin methods for elliptic problems with multiple scales, Lecture Notes in Computational Science and Engineering 44 (2005) 1–20.
[2] R. Ababou, D. McLaughlin, L.W. Gelhar, A.F.B. Tompson, Numerical simulation of three-dimensional saturated flow in randomly heterogeneous porous media, Transport in Porous Media 4 (1989) 549–565.
[3] G. Allaire, R. Brizzi, A multiscale finite element method for numerical homogenization, SIAM Multiscale Modeling and Simulation 4 (2005) 790–812.
[4] M. Barrault, Y. Maday, N.C. Nguyen, A.T. Patera, An empirical interpolation method: application to efficient reduced-basis discretization of partial differential equations, Comptes Rendus de l Academie des Sciences Paris, Serie I 339 (2004) 667–672.
[5] A. Bensoussan, J.L. Lions, G.C. Papanicolaou, Asymptotic Analysis for Periodic Structures, North-Holland, Amsterdam, 1978.
[6] S. Boyaval, Reduced-basis approach for homogenization beyond the periodic setting, SIAM Multiscale Modeling and Simulation 7 (1) (2008) 466–494.
[7] D.T. Burr, E.A. Sudicky, R.L. Naff, Nonreactive and reactive solute transport in three-dimensional heterogeneous porous media: mean displacement, plume spreading, and uncertainty, Water Resources Research 30 (1994) 791–816.
[8] Z. Chen, T.Y. Hou, A mixed multiscale finite element method for elliptic problems with oscillating coefficients, Mathematics of Computation 72 (242) (2003) 541–576.
[9] M.E. Cruz, A.T. Patera, A parallel Monte-Carlo finite-element procedure for the analysis of multicomponent random media, International Journal for Numerical Methods in Engineering 38 (1995) 1087–1121.
[10] C.N. Davies, Air Filtration, Academic Press, London, 1973.
[11] B.B. Dykaar, P.K. Kitanidis, Determination of the effective hydraulic conductivity for heterogeneous porous media using a numerical spectral approach: 1. Method, Water Resources Research 28 (1992) 1155–1166.
[12] B.R. Gebart, Permeability of unidirectional reinforcements for rtm, Journal of Composite Materials 26 (1992) 1100–1133.
[13] M.A. Grepl, N.C. Nguyen, K.Veroy, A.T. Patera, G.R. Liu, Certified rapid solution of parametrized partial differential equations for realtime applications, in: Proceedings of the 2nd Sandia Workshop of PDE-Constrained Optimization: Towards Real-Time and On-line PDE-Constrained Optimization, SIAM Computational Science and Engineering Book Series, 2007, pp. 197–212.
[14] P. Holmes, J.L. Lumley, G. Berkooz, Turbulence, Coherent Structures, Dynamical Systems and Symmetry, Cambridge University Press, 1996.
[15] T.Y. Hou, X.H. Wu, A multiscale finite element method for elliptic problems in composite materials and porous media, Journal of Computational Physics 134 (1) (1997) 169–189.
[16] T.Y. Hou, X. H Wu, Z. Cai, Convergence of a multiscale finite element method for elliptic problems with rapidly oscillating coefficients, Mathematics of Computation 68 (227) (1999) 913–943.
[17] P. Jenny, S.H. Lee, H.A. Tchelepi, Multiscale finite-volume method for elliptic problems in subsurface flow simulation, Journal of Computational Physics 187 (1) (2003) 47–67.
[18] J.R. Levick, Flow through interstitum and other fibrous matrices, Quarterly Journal of Experimental Physiology 72 (1987) 409–438.
[19] J.L. Lumley, The structure of inhomogeneous turbulent flows, in: A.M. Yaglom, V.I. Tatarski (Eds.), Atmospheric Turbulence and Radio Wave Propagation, Nauka, Moscow, 1967, pp. 166–178.
[20] Y. Maday, A.T. Patera, G. Turinici, A priori convergence theory for reduced-basis approximations of single-parameter elliptic partial differential equations, Journal of Scientific Computing 17 (1-4) (2002) 437–446.

[21] M. Meyer, H.G. Matthies, Efficient model reduction in non-linear dynamics using the karhunen-loeve expansion and dual-weighted-residual methods, Computational Mechanics 31 (1–2) (2003) 179–191.
[22] B.C. Moore, Principal component analysis in linear systems: controllability, observability, and model reduction, IEEE Transactions on Automatic Control 26 (1) (1981) 17–32.
[23] S. Moskow, M. Vogelius, First order corrections to the homogenized eigenvalues of a periodic composite medium. a convergence proof, Proceedings of the Royal Society of Edinburgh Section A 127 (1997) 1263–1299.
[24] N.C. Nguyen, A posteriori error estimation and basis adaptivity for reduced-basis approximation of nonaffine-parametrized linear elliptic partial differential equations, Journal of Computational Physics 227 (2007) 983–1006.
[25] N.C. Nguyen, K. Veroy, A.T. Patera, Certified real-time solution of parametrized partial differential equations, in: S. Yip (Ed.), Handbook of Materials Modeling, Springer, 2005, pp. 1523–1559.
[26] A.T. Patera, G. Rozza, Reduced basis approximation and a posteriori error estimation for parametrized PDEs, MIT-Pappalardo Graduate Monographs in Mechanical Engineering Series, Copyright MIT, 2006–2007. Available from: <http://augustine.mit.edu/methodology/methodology_book.htm>.
[27] C. Prud'homme, D. Rovas, K. Veroy, Y. Maday, A.T. Patera, G. Turinici, Reliable real-time solution of parametrized partial differential equations: reduced-basis output bound methods, Journal of Fluids Engineering 124 (1) (2002) 70–80.
[28] M.J.L. Robin, A.L. Gutjahr, E.A. Sudicky, J.L. Wilson, Cross-correlated random field generation with the direct fourier transform method, Water Resources Research 29 (1993) 2385–2398.
[29] G. Rozza, D.B.P. Huynh, A.T. Patera, Reduced basis approximation and a posteriori error estimation for affinely parametrized elliptic coercive partial differential equations: application to transport and continuum mechanics, Archives of Computational Methods in Engineering 25 (3) (2008) 229–275.
[30] S. Sen, K. Veroy, D.B.P. Huynh, S. Deparis, N.C. Nguyen, A.T. Patera, natural norm a posteriori error estimators for reduced basis approximations, Journal of Computational Physics 217 (2006) 37–62.
[31] L. Sirovich, Turbulence and the dynamics of coherent structures, part 1: Coherent structures, Quarterly of Applied Mathematics 45 (3) (1987) 561–571.
[32] A.F.B. Tompson, Numerical simulation of chemical migration in physically and chemically heterogeneous porous media, Water Resources Research 29 (1993) 3709–3726.